CONVECTIVE STAGNATION-POINT HEAT TRANSFER IN PARTIALLY EQUILIBRIUM FLOW OF HIGHLY IONIZED NITROGEN

Arthur F. Okuno* and Chul Park*

Ames Research Center, NASA, Moffett Field, Calif. 94035

ABSTRACT

Measurements of stagnation-point heat-transfer rate in a nitrogen stream at high ionization levels were made in a continuously operated arc-heated wind tunnel. The stream was thought to be frozen for molecular dissociation and in equilibrium for ionization in the boundary layer, and an analysis was made of this partially equilibrium flow. The results of both theory and experiment show that when the flow is partially in equilibrium, the total heat-transfer rate is appreciably lower than would be predicted by previous theories. The new theory provides a lower limit on heat-transfer rate attainable by a noncatalytic surface in the ionized regime.

INTRODUCTION

Measurements of stagnation-point heat-transfer rate in highly ionized nitrogen have been made in a shock tube by Rose and Stankevics.[1] Theoretical predictions,[2,3] based on the assumption of equilibrium flow, agreed well with the measurements. For continuously operated wind tunnels, in which most reentry heat shields are tested, the only available data for ionized flows were taken in an arc tunnel.[4] These data are preliminary, but they indicate that the heat-transfer rates may be considerably lower than those observed in a shock tube and may be lower than those predicted by the existing theories for either complete equilibrium or complete frozen flow. It is the purpose of the present work to confirm that the heat-transfer rate is indeed low when measured in a typical arc-heated wind tunnel and also to determine the cause of such a low heat-transfer rate.

The pressures required to operate an arc-heated wind tunnel produce a flow that, in general, is frozen for molecular dissociation and in equilibrium for ionization in the boundary layer. The rate of heat transfer at the stagnation point of a hemisphere is measured in this frozen-dissociated and equilibrium-ionized flow and is compared with the theoretical values calculated for this partially equilibrium flow. For the determination of the stream enthalpy, which was the major uncertainty in the data for ionized flows shown in Ref. 4, a spectroscopic technique was used.

ANALYSIS

Basic Equations

Mass and momentum. The equations of conservation of mass and momentum in the boundary layer at the stagnation point of an axisymmetric blunt body are well known. Taking the coordinate system as shown in Fig. 1, they are

$$\text{(Mass)} \qquad \frac{\partial}{\partial x}(\rho u x) + \frac{\partial}{\partial y}(\rho v y) + \frac{\rho v y}{R} = 0 \tag{1}$$

$$\text{(Momentum)} \qquad \rho\left(u\frac{\partial u}{\partial x} + v\frac{\partial u}{\partial y}\right) = \frac{\partial}{\partial y}\left(\mu\frac{\partial u}{\partial y}\right) - \frac{\partial p}{\partial x} \tag{2}$$

*Research Scientist.

The above equations are reduced to dimensionless form through the following transformation of variables.

$$\left.\begin{aligned} \xi &= \int_0^x \rho_e \mu_e u_e x^2 \, dx , \qquad \eta = \frac{u_e}{\sqrt{2\xi}} \int_0^y \rho x \, dy \\ \frac{\partial \psi}{\partial y} &= \rho u x , \qquad -\frac{\partial \psi}{\partial x} = \rho v x , \qquad \psi = \sqrt{2\xi}\, f(\eta) \end{aligned}\right\} \tag{3}$$

where $u_e = (du_e/dx)_o x$. Equations (1) and (2) are then combined into a single dimensionless equation, which is, at the stagnation point,

$$\left(\frac{f''}{a}\right)' + ff'' + \frac{1}{2}\left(\frac{\rho_e}{\rho} - f'^2\right) = 0 \tag{4}$$

where the prime denotes the differentiation with respect to η. The boundary conditions are

$$\eta = 0 , \quad f = f' = 0 ; \quad \eta = \infty , \quad f' = 1 \tag{5}$$

Species. In general, there are five different species in nitrogen for temperatures up to 20,000° K. They are N_2, N_2^+, N, N^+, and e. Among these, the condition of charge neutrality requires that the number of positive and negative charges be the same, i.e.,

$$n(N_2^+) + n(N^+) = n(e) \tag{6}$$

in which $n()$ denotes the number density, cm^{-3}, of species specified within the parentheses.

The concentration of each species in the boundary layer is governed by the equation of species conservation

$$\rho\left(u \frac{\partial C_i}{\partial x} + v \frac{\partial C_i}{\partial y}\right) = \frac{\partial}{\partial y}\left(\rho D_i \frac{\partial C_i}{\partial y}\right) + w_i \tag{7}$$

where D_i is an appropriately defined diffusivity[5] yet to be specified. By transforming the coordinates in accordance with Eqs. (3), Eq. (7) becomes

$$\left(\frac{C_i'}{b_i}\right)' + fC_i' = \frac{w_i}{2(du_e/dx)_o} \tag{8}$$

For the dissociation reaction

$$N_2 + M \rightleftarrows N + N + M \quad \begin{matrix}(\text{Collisional dissociation and} \\ \text{three-body recombination})\end{matrix} \tag{9}$$

where M designates an arbitrary third body, the rate coefficient is of the order of 10^{15} cm^6 $mole^{-2}$ sec^{-1} for recombination.[6] For pressures below 1 atm and a nose radius of 1.27 cm, the RHS (right-hand side) of Eq. (8) is always much smaller than unity for this dissociation reaction. The RHS of Eq. (8) is neglected for reaction (9), that is, dissociation is assumed to be frozen for the conditions of interest. For the ionization process

$$N + e \rightleftarrows N^+ + e + e \quad \begin{matrix}(\text{Collisional ionization and} \\ \text{three-body recombination})\end{matrix} \tag{10}$$

the rate coefficient is derived by Park[7] as being approximately $1.15 \times 10^{-26}(T/10{,}000)^{-5.27}$ cm^6 sec^{-1}. The reaction rate w can be written for

this case; therefore,

$$w(N^+) = 1.15\times10^{-26}\left(\frac{T}{10{,}000}\right)^{-5.27} n(N^+)n(e)^2\left[\frac{n(N)}{n_E(N)} - 1\right]$$

in which

$$n_E(N) = n(e)^2 \frac{Z_p}{2Z_{p+}}\left(\frac{h_p^2}{2\pi mkT}\right)^{3/2} e^{E_\infty/kT} \tag{11}$$

The stagnation-point velocity gradient $(du_e/dx)_o$ in the present test conditions is found, using the modified Newtonian approximation, to be 0.405×10^6 sec^{-1} ± 20%. The species equation for the process (10) is therefore approximately

$$\left\{\frac{[n(N^+)]'}{b}\right\}' + f[n(N^+)]' \simeq D_a n(N^+)\left[\frac{n(N)}{n_E(N)} - 1\right]$$

where

$$D_a = 1.41\times10^{-32} n(e)^2 (T/10{,}000)^{-5.27} \tag{12}$$

The Damkoehler number, D_a, is found to be greater than unity at and near the boundary-layer edge for all the conditions studied in the present work. When the Damkoehler number is larger than unity, the flow is in near equilibrium. For simplicity, therefore, the flow is assumed to be in equilibrium for process (10). This assumption breaks down in the low-temperature region near the wall where the temperature, and hence electron density, is low. Fortunately, in this low-temperature region, there is molecular species N_2 present which acts as a catalyst. In the presence of N_2, species N^+ can be removed through the process

$$N^+ + N_2 \rightarrow N_2^+ + N \qquad \text{(Charge exchange)} \tag{13}$$

$$N_2^+ + e \rightarrow N + N \qquad \text{(Dissociative recombination)} \tag{14}$$

Because these are two-body processes and because they have large cross sections,[8] the absolute rate of removal of N^+ will be large even when the concentration of N_2 is small. For this reason, the assumption of equilibrium for process (10) is used throughout the boundary layer.

The species N_2^+ can be formed through either charge exchange with atomic ions, process (13), or direct collisional ionization:

$$N_2 + e \rightarrow N_2^+ + e + e \qquad \text{(Collisional ionization)} \tag{15}$$

However, the rate of disappearance, process (14), is so large[8] that in the steady state, the absolute concentration of N_2^+ is negligibly small compared to the concentration of N^+. Because the elastic cross section of N_2^+ is not much different from that of N^+,[9] a small percentage of N_2^+ does not affect the transport properties. Therefore, the concentration of N_2^+ is neglected completely, i.e., $n(N_2^+) = 0$.

Because there are four species and because Eq. (6) and the equation of state impose two conditions, one needs only two parameters to define the composition of the gas. These are the ionization fraction α and dissociation fraction β defined as

$$\alpha = \frac{n(N^+)}{n(N) + n(N^+)} \quad ; \quad \beta = \frac{n(N)}{2n(N_2) + n(N)} \tag{16}$$

The foregoing considerations lead to the concept of a "partially equilibrium" ionized gas, or more specifically "equilibrium-ionization, frozen-dissociation" gas model. The gas is considered to be in equilibrium at and near the edge of the boundary layer. In this region, there can be no molecular species N_2 because they are removed through processes (13) and (14). At a certain point within the boundary layer, the temperature will be such that the degree of ionization is zero. Between this point and the wall, there are only the neutral species N and N_2. Because the dissociation reaction is frozen, species N_2 can be created only at the wall through surface recombination. The surface between the two regions will be called "interface" and will be denoted by the subscript m. The region between the interface and the wall will be called "dissociated sublayer." For the purposes of computation, the interface is taken as the point where the equilibrium degree of ionization becomes 0.1%.

The species Eq. (8) is replaced in the ionized region by the Saha equation which can be written approximately in dimensionless form as[10]

$$\frac{\alpha^2}{1-\alpha} = \frac{\rho_c}{\rho}\left(\frac{T}{T_c}\right)^{5/2} \exp\left(-\frac{T_c}{T}\right)$$

In the dissociated sublayer, the species Eq. (8) becomes

$$\left(\frac{\beta'}{b}\right)' + f\beta' = 0 \tag{17}$$

The diffusivity, D, in the parameter b is now identical to that in the work of Goulard.[11] At the wall, linear surface catalytic reaction rate is assumed.[11] This gives the boundary condition at the wall

$$\beta'(0) = (\rho_e \mu_e)^{1/2}\left[2\left(\frac{du_e}{dx}\right)_o\right]^{-1/2} \frac{kw}{\rho_w D_w}\beta(0) \tag{18}$$

The other boundary condition for Eq. (17) is given at the interface,

$$\beta(\eta_m) = 1 \tag{19}$$

Energy. Two separate energy equations are needed for the two distinct regions. For the equilibrium-ionized region, the formulation of DeRienzo and Pallone[3] is adopted because it is simple, and because the results of computations by DeRienzo and Pallone agree closely with those of Fay and Kemp[2] who used a more complex gas model. Thus the energy equation in ionized regions is

$$\left(\frac{H'}{c}\right)' + fH' = 0 \tag{20}$$

The boundary conditions are:

$$\eta = \eta_m\ , \quad H' = H'_m\ ; \quad \eta = \infty\ , \quad H = H_e \tag{21}$$

The enthalpy H in the ionizing regime is expressed as

$$H = \left[2.5(1+\alpha)\frac{T}{T_c} + \alpha\right] h_c + h_d$$

For the dissociated sublayer regime, the formulation of Goulard[11] is followed. The Lewis number is assumed to be unity. This results in an energy equation identical to Eq. (20) in appearance. The parameter c in Eq. (20) reduces

to b of Eq. (8) for this case. The boundary conditions are

$$\eta = 0 , \quad H = H_w ; \quad \eta = \eta_m , \quad H' = H'_m \tag{22}$$

The enthalpy is calculated assuming that vibration is fully excited and frozen at the value at the interface.

Transport Properties

Ionized regime. The transport properties for nitrogen required for the solution of differential Eqs. (4), (17), and (20) must be defined so that they are consistent with the derivations of the respective differential equations. For the equilibrium-ionized regime, the present analysis is identical to that in Ref. 3; therefore, the transport properties are taken from the same source. The transport properties are derived from Refs. 9 and 12, where they are given for pressures of 1 atm and greater, by extrapolating to a pressure of 0.1 atm for the present study.

Figure 2 is a plot of $\mu(1000/T)$ against the compressibility Z. As seen from the figure, the parameter $\mu(1000/T)$ is a function mainly of Z and is a weak function of pressure. For pressures below 1 atm, therefore, the viscosity is approximated by the dashed line,

$$\mu = 2.66\times10^{-7} \times 13.3^{-\alpha_T} , \quad \text{poise} \qquad Z > 2 \tag{23}$$

In order to solve the energy equation, it is necessary to know the ratio of K/c_p. Unfortunately, Ref. 12 does not present correct, explicit values of K or c_p. However, they are shown in Ref. 3 in graphical form and in the present work are read from these graphs. Figure 3 shows the variation of $(K/c_p)(1000/T)^2$ against Z. The parameter K/c_p is approximated for pressure below 1 atm by

$$\frac{K}{c_p} = 2.97 \times 1.329^{\frac{1}{0.103+\alpha}}\times10^{-6} \left(\frac{T}{1000}\right)^2 , \quad \text{cm}^{-1}\,\text{g}^{-1}\,\text{sec}^{-1} \qquad Z > 2 \tag{24}$$

Equation (24) is shown in Fig. 3. As seen from the figure, as Z approaches 2, Eq. (24) approaches the curve for the frozen dissociated regime derived from Eqs. (25) and (26). The discrepancy between the present values and those of Ref. 12 at Z = 2 is due to the difference in the assumed chemistry. The data in Ref. 12 are for equilibrium dissociation while the present analysis assumes the dissociation to be frozen.

Dissociated regime. For the dissociated regime, the formulation is for a frozen flow and therefore the frozen transport properties are required. The frozen thermal conductivity is taken from Ref. 2 as

$$K = K_A \frac{0.72 + 1.28\beta}{1 + \beta} , \qquad Z < 2 \tag{25}$$

where

$$K_A = 3.51\times10^{-6}T^{0.81} , \qquad \text{W cm}^{-1}\,{}^{\circ}\text{K}^{-1}$$

Because the vibrational energy is assumed to be fully excited at the value at the interface, the (frozen) specific heat becomes

$$c_p = 5\mathcal{R} = 1.479 , \quad \text{Jg}^{-1}\,{}^{\circ}\text{K}^{-1} \qquad Z < 2 \tag{26}$$

he Prandtl number is assumed to be 0.713. The viscosity is derived from Eqs. (25), (26), and the condition that Prandtl number is 0.713. Lewis number is assumed to be unity.

At $Z = 2$, a transport property calculated for the dissociated sublayer must match that calculated for the ionized layer. Because the transport properties determined by Eqs. (23) to (26) do not match exactly at point $Z = 2$, an arbitrary machine fairing was applied at around $Z = 2$ as shown in Figs. 2 and 3.

EXPERIMENTAL APPARATUS AND TESTING PROCEDURE

The wind tunnel was the constricted-arc type[13] and had a constrictor 1.27 cm in diameter and 30.5 cm long, followed by a diverging contoured nozzle of area ratio 22 (Fig. 4).

The heat-transfer rates to the stagnation region of a hemisphere-cylinder with base diameter of 2.54 cm were measured with a heat-sink transient-type calorimeter (Fig. 5). The copper calorimeter slug was 0.475 cm in diameter and 0.5 cm long. Both the calorimeter slug and shroud were coated with nickel.

The calorimeter was inserted into the center line of the stream for prescribed times and was shielded during insertion and retraction from the stream. Details of the method used to determine the heat-transfer rate from the temperature variation of the calorimeter slug are given in Ref. 14. The stagnation-point pressures were measured with a 2.54-cm-diameter water-cooled hemisphere-cylinder probe which had a 0.318-cm-diameter orifice at the stagnation point connected to a strain-gage-type pressure transducer. The range of stagnation pressures was 0.1 to 0.25 atm.

The enthalpy of the plasma stream in the stagnation region was determined spectroscopically from the intensities of spectral lines radiated from the stagnation shock layer.[15] A spectrograph was focused on the center-line stagnation region of the shock layer. The intensity ratio of lines varies typically as shown schematically in Fig. 6. The plateau of the intensity ratio shown in the figure between the shock-wave overshoot and boundary-layer region corresponds to the equilibrium, inviscid region of the flow. In the present test, it was found that at pressures approximately equal to and above 0.1 atm, the shock-wave overshoot was negligibly small in magnitude and width and therefore the plateau was well defined. An ion-atom intensity ratio method[15] was used to determine the state condition in the inviscid region whenever the ion line was measurably strong, that is, for temperatures above approximately 14,000° K. For the lower range of enthalpies where the ion line was not measurable, an atom-atom line intensity ratio was used. The spectral lines chosen were 5680 NII, 6008 NI, and 7468 NI. The oscillator strengths of the lines 5680 NII and 7468 NI were taken from Refs. 16 and 17 as 0.43 and 0.089. The oscillator strength of the line 6008 NI was determined experimentally by comparing with the other two lines as follows.

Because the ion-atom intensity ratio method yields a temperature that is quite insensitive to the error in the oscillator strengths,[15] the temperature can be determined accurately by the ion-atom ratio method without the knowledge of the exact values of oscillator strengths. The temperature was first determined for the high-enthalpy region from the ratios of 5680 NII vs. 7468 NI and 5680 NII vs. 6008 NI. The oscillator strength of 6008 NI was taken from the Coulomb approximation[18] for this purpose. The inverse of the resulting temperature was plotted against the ratio of line 6008 NI vs. 7468 NI. Then the best fit logarithmic curve was determined from this plot. This procedure yields 0.0435 as the most probable oscillator strength of line 6008 NI, but this value is subject to uncertainty because 7468 NI was used as the reference oscillator

strength. Nevertheless, it was considered sufficiently accurate for the present application, because it provides a value calibrated against an accurate measurement at the same condition.

A 2.25-meter spectrograph was used for the present test. The intensities of the three lines were detected by three photomultiplier tubes. The entrance and exit slits were 50 and 500 microns wide, respectively. Because of the relatively wide exit slit, the contribution of continuum background was not negligible and was therefore calculated theoretically and subtracted from the measured line intensities. The continuum was considered to originate from the free-bound transitions into the atomic nitrogen states of principal quantum numbers 3 and 4, and free-free transition (Bremstrahlung). The Gaunt factors for the free-bound transition into the states of principal quantum number 3 were taken from Ref. 19. The Gaunt factors for the free-bound transition into the states of principal quantum number 4 and free-free Gaunt factors were assumed to be the same as for hydrogen.[18] The calculation of temperature from the measured intensity ratios and stagnation pressure requires an iteration. This iterative calculation was performed on a digital computer.

Enthalpy was then determined from the temperature and impact pressure. A scatter of approximately ±3% was found in the enthalpy values resulting from the ion-atom line ratio and ±15% from the atom-atom line ratio.

DISCUSSION OF RESULTS

Boundary-layer Eqs. (4), (17), and (20) with the boundary conditions (5), (21), and (22) and expressions for the transport properties were solved numerically on a digital computer for pressures of 0.1 and 1.0 atm and for various surface catalytic reaction-rate constants for atomic recombination. The surface temperature was assumed to be 500° K. The results of the analysis for a partially equilibrium flow are shown in Fig. 7. The ordinate is the heat-transfer rate normalized by $(R/p_s)^{1/2}$ and the abscissa is the total enthalpy. The lowest curves are for a noncatalytic surface, $k_w = 0$, and give the minimum possible heat-transfer rate because no atoms recombine at the surface and the chemical energy remains in the gas. The highest curves are for a fully catalytic surface, $k_w = \infty$, and give the maximum possible heat-transfer rate because all the atoms recombine at the surface. The intermediate curves are for surfaces with k_w = 1,000 and 10,000 cm/sec. Although not shown, the computations were repeated for a surface temperature of 300° K for a limited number of cases. No difference was found between the heat-transfer rates for surface temperatures of 300° and 500° K.

Since the heat-transfer rate to a surface with k_w = 1000 cm/sec is only about 10% higher than to a noncatalytic surface, and since for most materials k_w is lower than 1000 cm/sec,[4,11] the type of surface does not appreciably affect the heat-transfer rate for a nose radius of 1.27 cm and a pressure of 0.1 atm. It can be shown that the recombination heat-transfer rate is a function only of the product $k_w\sqrt{p_s R}$, that is,

$$\frac{q - q_{k_w=0}}{q_{k_w=\infty} - q_{k_w=0}} = f(k_w\sqrt{p_s R}) \tag{27}$$

By use of this relationship, shown in Fig. 8, the present theoretical results can be extended to different pressures and nose radii. For flight conditions, for a finite k_w, the heat-transfer rate can vary over a wide range between the minimum, $q_{k_w=0}$, and maximum, $q_{k_w=\infty}$, depending on the pressure and nose radius.

In Fig. 9, the present analysis for a stagnation pressure of 1 atm is compared with the theories of Fay and Kemp[2] and DeRienzo and Pallone.[3] The normalized heat-transfer rate to a noncatalytic surface is less than predicted by the other theories. For a fully catalytic surface, the normalized heat-transfer rate is roughly the same as that calculated by Fay and Kemp[2] for frozen flow, in which the wall is considered to be fully catalytic. It is seen from Fig. 9 that the effect of surface catalysis for atomic recombination is surprisingly large. From Goulard's theory[11] one would expect that the ratio of the atomic recombination heat-transfer rate to conductive heat-transfer rate would be equal to the ratio of the heat of dissociation to frozen enthalpy, that is, $(q_r/q_c)_{max} = h_d/H_f \equiv h_d/(H-h_d)$. Instead, the present analytical results can be correlated approximately by

$$\left(\frac{q_r}{q_c}\right)_{max} \equiv \frac{q_{k_w=\infty} - q_{k_w=0}}{q_{k_w=0}} \simeq \frac{h_d}{H_f}\sqrt{\frac{\mu_m}{\mu_e}} \tag{28}$$

That is, the ratio of the two heat-transfer rates is greater than expected from Goulard's theory[11] by a factor of $(\mu_m/\mu_e)^{1/2}$. Mathematically, this increase can be explained as follows. For the present ionized flow, it can be shown from the definition of heat-transfer rates that when $k_w = \infty$, the ratio of heat-transfer rates can be expressed as

$$\left(\frac{q_r}{q_c}\right)_{max} = \frac{\sigma}{S_c}\frac{h_d(d\beta/dy)_w}{(dH_f/dy)_w} \simeq \frac{h_d}{H_f}\frac{\delta_e}{\delta_m}$$

Since $\delta_e \sim \mu_e^{-1/2}$ and $\delta_m \sim \mu_m^{-1/2}$, Eq. (28) is obtained.

A physical explanation of this increase in recombination heat transfer is as follows. When the flow is ionized, the Reynolds number increases and the Prandtl number decreases. These two effects oppose each other and so δ_e is essentially unchanged. The interface thickness δ_m, however, is affected only by the Reynolds number and is therefore reduced, resulting in a steeper atom concentration profile gradient at the wall.

Measured heat-transfer rates are shown in Fig. 10. Compared with the shock-tube data of Ref. 1, which are not shown, the present experimental results are lower by approximately 25% in the mean. The discrepancy would be expected because of the differences in boundary-layer chemistry between the two experiments. In the experiments of Ref. 1, the stagnation-point pressure was greater than 7 atm, so the flow was in equilibrium for both ionization and dissociation. As seen from Figs. 7 and 9, one would expect a higher heat-transfer rate from a completely equilibrium flow than from the partially equilibrium flow. Pope's data[4] are shown in the same figure where the enthalpy was corrected by about 10% on the basis of present enthalpy measurements. Although Pope's measurements were taken at pressures of 0.05 to 0.08 atm with a model of nose radius 4.6 cm, the $k_w\sqrt{p_s R}$ parameter is about the same as that of the present tests, and therefore the agreement of the data is to be expected.

Also shown in Fig. 10 are the heat-transfer-rate curves predicted for a noncatalytic surface, $k_w = 0$, and a fully catalytic surface, $k_w = \infty$. The slope of the mean value of the experimental points is greater than the slopes of predicted curves for a constant reaction rate. This difference in slope probably occurs because the present theory assumes complete equilibrium ionization and therefore allows for no penetration of the electrons below the interface. In the actual case, the electrons penetrate below the interface because the recombination rate is finite. Therefore, the real electron density profiles would tend to lie between those of the present theory and that of Fay and Kemp[2] for

frozen flow in which both ionization and dissociation are assumed to be frozen. Accordingly, one would expect the slope of the heat-transfer rate versus enthalpy curve to lie between those of the two theories.

For the present test conditions in which ionization is near equilibrium, an empirical curve providing the best fit for the experimental points is

$$q\sqrt{R/p_s} = -2.4\times10^6 + 0.096H_\infty , \qquad 90\times10^6 < H_\infty < 175\times10^6 \tag{29}$$

where q is the heat-transfer rate in watts/meter^2, H_∞ is the total stream enthalpy in joules/kilogram, p_s is the stagnation-point pressure in atmospheres, R is the nose radius in meters. The conditions for the applicability of the formula are that the Damkoehler number for ionic recombination in the boundary layer be larger than 1; the Damkoehler number for the atomic recombination be much smaller than 1; parameter $k_w\sqrt{p_s R}$ be between 150 and 300; and the enthalpy be within the stated limits. If the above conditions are satisfied, the empirical equation can be used to determine the enthalpy from the heat-transfer rate without a direct measurement of enthalpy.

CONCLUSIONS

The heat-transfer rates measured in an arc-heated wind tunnel in an ionized flow were about 25% lower than those taken in a shock tube. The present results are explained by the partially equilibrium (frozen-dissociation and equilibrium-ionization) flow in the wind tunnel. In this type of flow, a surface which is noncatalytic to atomic recombination can reduce the heat-transfer rate by an amount equal to $(\mu_m/\mu_e)^{1/2}$ times the value predicted by the theory of Goulard. The present analysis of a partially equilibrium flow tends to underestimate the measured results slightly in the highly ionized regime. An empirical heat-transfer-rate formula is given that can be used for determining stream enthalpy in the absence of a direct measurement of the enthalpy.

NOMENCLATURE

a	$\frac{\rho_e\mu_e}{\rho\mu}$
b	$\frac{\rho_e\mu_e}{\rho\mu} S_c$
C_i	species i
c	$\frac{\rho_e\mu_e}{\rho\mu} \sigma$
c_p	specific heat
D	diffusion coefficient
D_a	Damkoehler number (Eq. (12))
D_i	multicomponent diffusion coefficient for species i
$\left(\frac{du_e}{dx}\right)_o$	stagnation-point velocity gradient at edge of boundary layer
E_∞	effective ionization potential of neutral atoms
e	electron
H	total enthalpy

H_f	$H - h_d$
h_c	characteristic energy of ionization for nitrogen, 1.00125×10^5 Jg^{-1}
h_d	dissociation energy for nitrogen, 3.3591×10^4 Jg^{-1}
h_p	Planck's constant
K	thermal conductivity
k	Boltzmann constant
k_w	surface catalytic atomic recombination rate constant, cm sec^{-1}
m	electron mass
N	neutral atom
N^+	ionized atom
N_2	neutral molecule
N_2^+	ionized molecule
n()	number density
$n_E(N)$	equilibrium number density of neutral atom (Eq. (11))
p	pressure
q	heat-transfer rate
R	radius
$\mathcal{R}$	gas constant
S_c	Schmidt number $\frac{\mu}{\rho D}$
T	temperature
T_c	characteristic temperature of ionization for nitrogen, $168{,}621^\circ$ K (Ref. 10)
u,v	x and y component of velocity, respectively
V_∞	free-stream velocity
w_i	rate of production of species C_i
x,y	distance parallel and perpendicular to wall, respectively
Z	compressibility factor
Z_p, Z_{p+}	partition function for neutral and ionized atoms, respectively
α, β	ionization and dissociation fraction, respectively (Eq. (16))
δ	boundary-layer thickness

μ viscosity

ρ density

ρ_c characteristic density of ionization for nitrogen, 14.59 g cm^{-3} (Ref. 10)

ξ,η dimensionless coordinate in x and y directions, respectively (Eq. (3))

σ Prandtl number, $\frac{\mu c_p}{K}$

Subscripts

e condition at edge of boundary layer

i dummy variable

m condition at interface

s inviscid stagnation region

w condition at wall

REFERENCES

1. Rose, P. H., and Stankevics, J. O. Stagnation-Point Heat-Transfer Measurements in Partially Ionized Air, AIAA J., 1963, 1, 2752-2763.
2. Fay, J. A., and Kemp, N. H. Theory of Stagnation-Point Heat Transfer in a Partially Ionized Diatomic Gas, AIAA J., 1963, 1, 2741-2751.
3. DeRienzo, P., and Pallone, A. J. Convective Stagnation-Point Heating for Re-entry Speeds up to 70,000 fps Including Effects of Large Blowing Rates, AIAA J., 1967, 5, 193-200.
4. Pope, R. B. Stagnation-Point Convective Heat Transfer in Frozen Boundary Layers, AIAA Paper 68-15, 1968.
5. Hirschfelder, J. O., Curtis, C. F., and Bird, R. B. Molecular Theory of Gases and Liquids, Chap. 8. New York: Wiley and Sons, 1954.
6. Eschenroeder, A. Q., Daiber, J. W., Golian, T. C., and Hertzberg, A. Shock tunnel studies of high enthalpy ionized airflows. In W. C. Nelson, ed., The High Temperature Aspects of Hypersonic Flow (AGARDograph 68). Pergamon Press, 1964, 217-254.
7. Park, C. Measurement of Ionic Recombination Rate of Nitrogen, AIAA Paper 67-703, 1967.
8. Nawrocki, P. J., and Papa, R. Atmospheric Processes, Chap. 3, Section 10. Prentice-Hall, 1963.
9. Yos, J. M. Transport properties of nitrogen, hydrogen, oxygen, and air to 30,000° K. AVCO/RAD-TM-63-7, March 1963.
10. Bray, K. N. C. Electron-ion recombination in argon flowing through a supersonic nozzle. In W. C. Nelson, ed., The High Temperature Aspects of Hypersonic Flow (AGARDograph 68). Pergamon Press, 1964, 67-87.
11. Goulard, R. On Catalytic Recombination Rates in Hypersonic Stagnation Heat Transfer, Jet Propulsion, 1958, 28, 737-745.
12. Bennett, S., Yos, J. M., Knopp, C. F., Morris, J., and Bade, W. L. Theoretical and experimental studies of high-temperature gas transport properties, final report. AVCO/RAD-SR-65-35, February 1965.

13. Shepard, C. E., Watson, V. R., and Stine, H. A. "Evaluation of a Constricted Arc Supersonic Jet," NASA TN D-2066, 1964.

14. Hiester, N. K., and Clark, C. F. "Feasibility of Standard Evaluation Procedures for Ablating Materials," NASA CR-379, 1966.

15. Park, C., and Okuno, A. F. "Diagnosis of High-Density Highly Ionized Nitrogen Wind Tunnel Flows," Proceedings of 2nd International Congress on Instrumentation in Aerospace Simulation Facilities, Stanford University, August 1966.

16. Mastrup, F., and Wiese, W. Experimentelle Bestimung der Oszillatorenstärken einiger NII - und OII Linien, Z. Astrophys., 1958, 44, 259-279.

17. Wiese, W. L., Smith, M. W., and Glennon, B. M. "Atomic Transition Probabilities, Vol. 1, Hydrogen through Neon," NSRDS-NBS 4, National Bureau of Standards, May 1966.

18. Griem, H. R. Plasma Spectroscopy. New York: McGraw-Hill, 1964.

19. Anderson, A. D., and Griem, H. R. "Continuum Emission Coefficients from the Quantum Defect Method," Proceedings of the 6th International Conference on Ionization Phenomena in Gases, Paris, 1963, 3, 293-295.

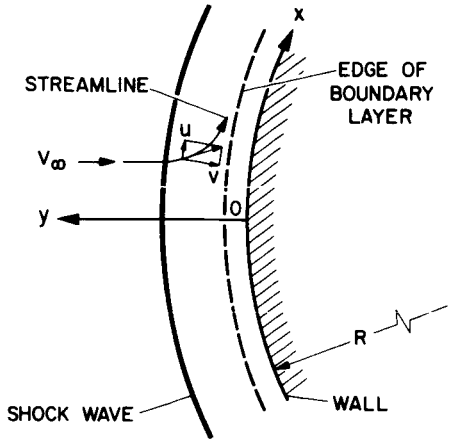

FIG. 1. Sketch of Flow Field in the Stagnation Region of an Axisymmetric Hypersonic Shock Layer.

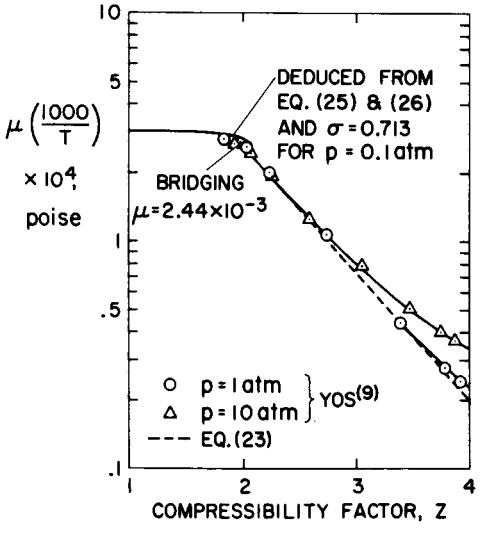

FIG. 2. Viscosity of Partially Equilibrium Nitrogen.

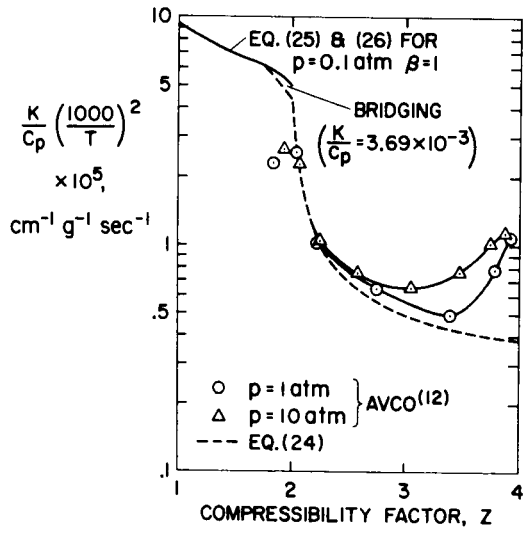

FIG. 3. K/c_p Ratio for Partially Equilibrium Nitrogen.

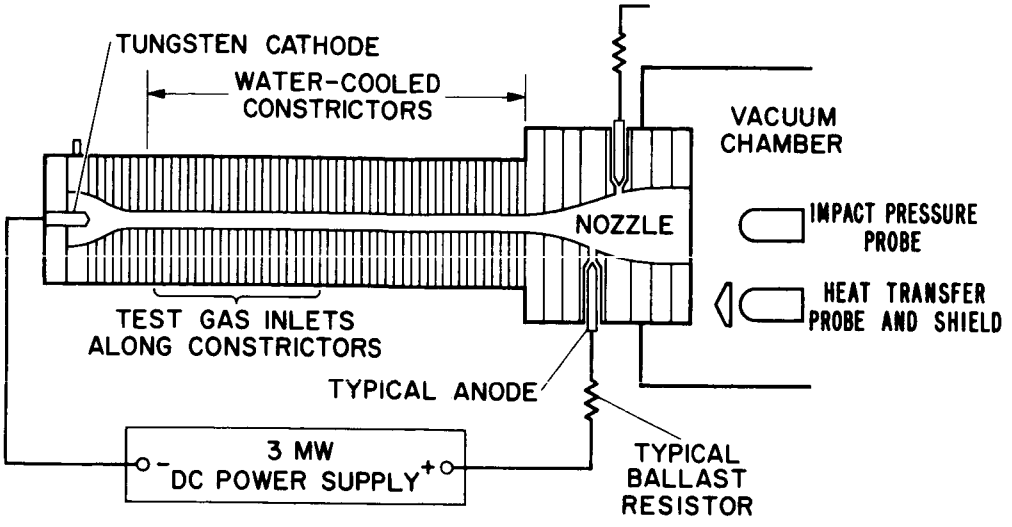

FIG. 4. Schematic Drawing of Constricted-Arc Wind Tunnel.

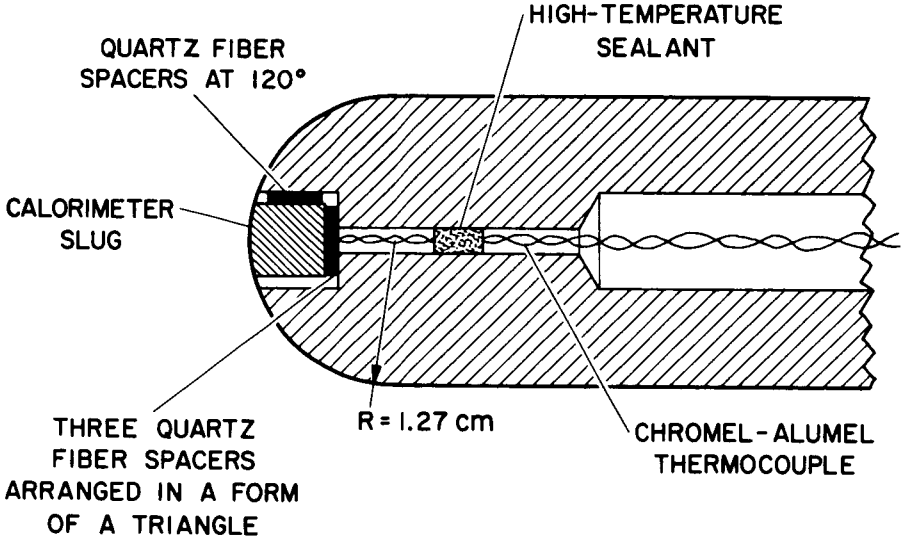

FIG. 5. Schematic Drawing of a Calorimeter.

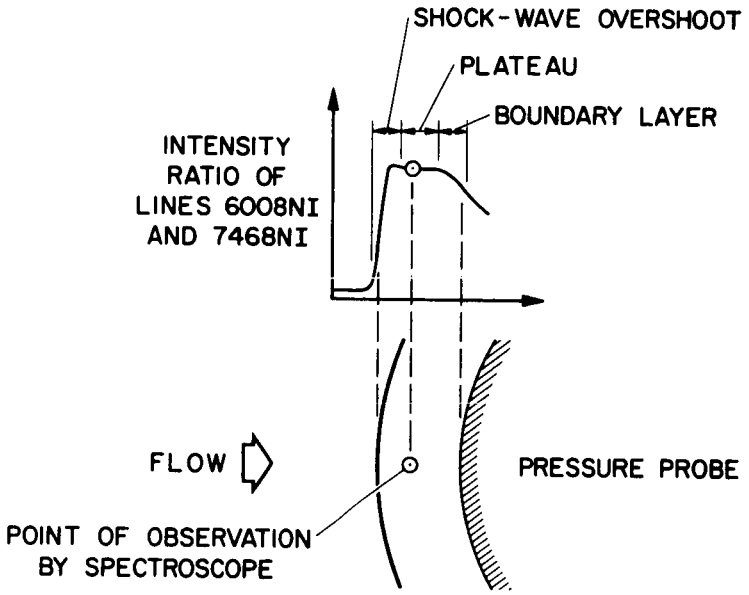

FIG. 6. Typical Variation of Intensity Ratio of Lines 6008NI vs. 7468NI as Observed by a Spectrograph Across the Stagnation-Region Shock Layer.

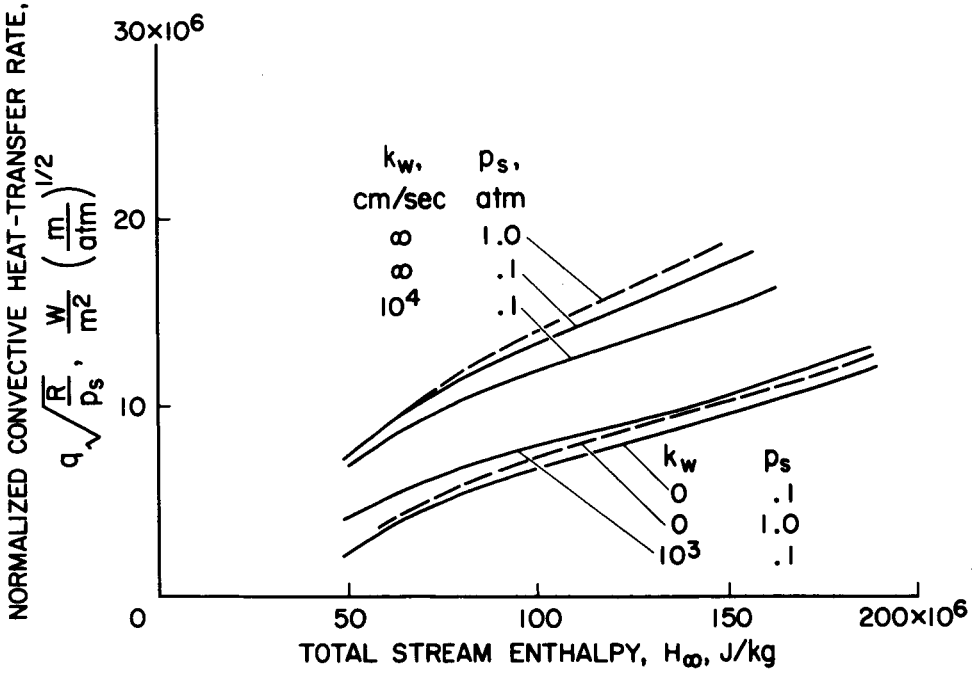

FIG. 7. Results of Analysis of Heat-Transfer Rate in an Equilibrium-Ionized and Frozen-Dissociated Nitrogen Stream.

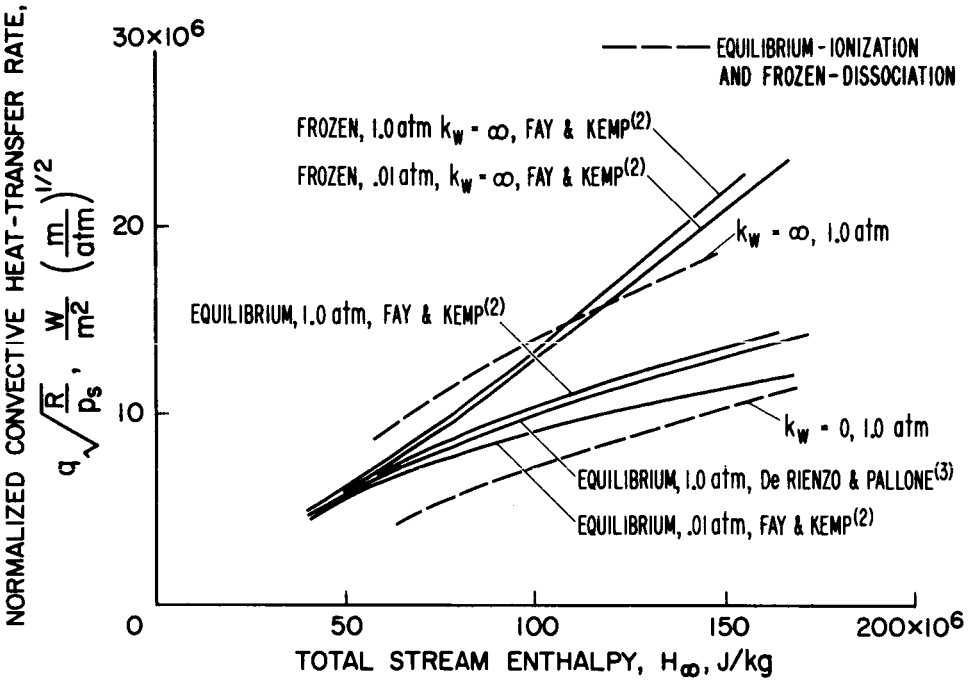

FIG. 9 Comparison of Calculations for Stagnation-Point Heat-Transfer Rate in Ionized Nitrogen.

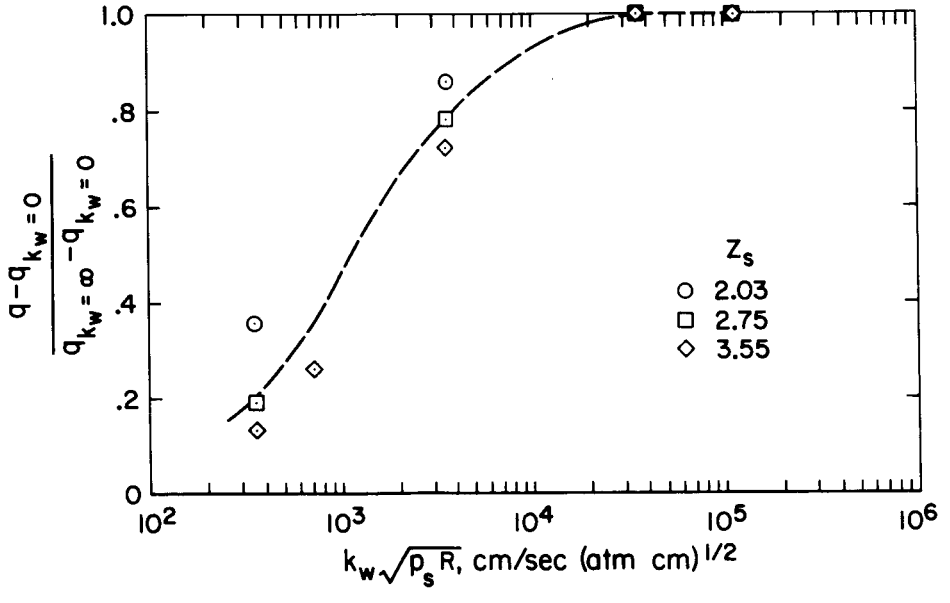

FIG. 8. Effect of Catalycity, Body Size, and Stagnation Pressure on Recombination Heat-Transfer Rate.

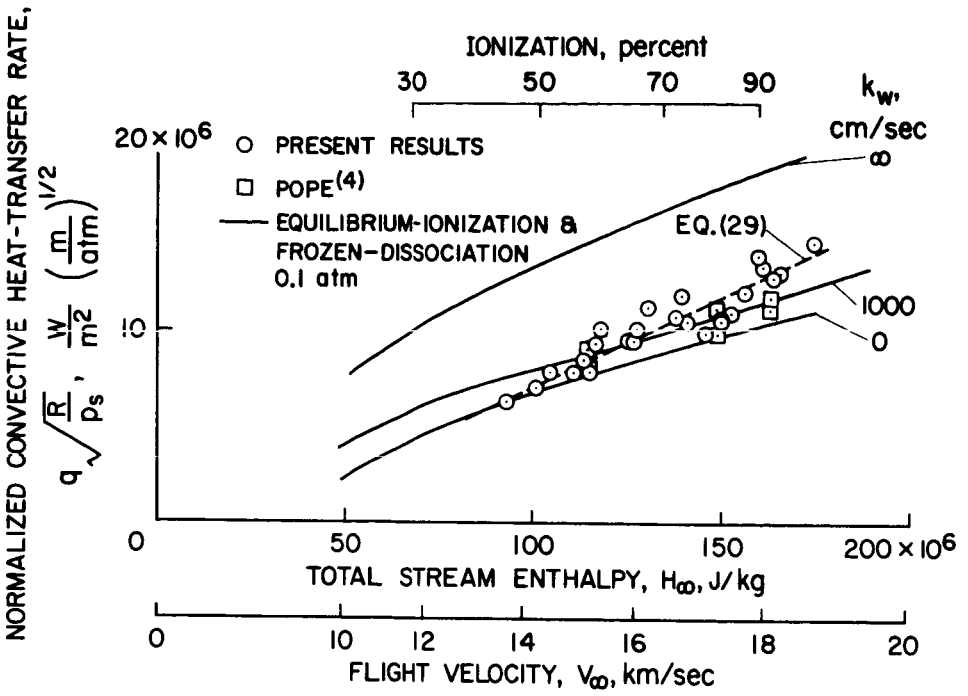

FIG. 10. Heat-Transfer Rate to Nickel Surfaces in Ionized Flows of Nitrogen.